Journal of Applied Polymer Science

Influence of fillers dispersion on friction and wear performance of solution styrene butadiene rubber composites

Yanping Wu,[1,2,3] Yang Zhou,[2] Jinlong Li,[2] Huidi Zhou,[1] Haichao Zhao,[2] Jianmin Chen[1,2,3]

[1]State Key Laboratory of Solid Lubrication, Lanzhou Institute of Chemical Physics, Chinese Academy of Sciences, Lanzhou 730000, China

[2]Key Laboratory of Marine Materials and Related Technologies, Zhejiang Key Laboratory of Marine Materials and Protective Technologies, Ningbo Institute of Materials Technology and Engineering, Chinese Academy of Sciences, Ningbo 315201, China

[3]Graduate School of Chinese Academy of Sciences, Beijing 100049, China

Correspondence to: J. Chen (E-mail: chenjm@licp.cas.cn)

ABSTRACT: Development of structure–properties relationships between the fillers/rubber matrix interface chemistry and the dispersion and interfacial adhesion properties of the rubber composites is critical to predict their bulk mechanical and tribological properties. In this paper, three solution styrene butadiene rubber (SSBR) composites containing various fillers with tailored interfacial chemistry were prepared via conventional mixing technique. Subsequently, thermal and structural features of filled SSBR composites were monitored by TG, DSC, XRD, XPS, FESEM and TEM, respectively. Sliding contact experiments were conducted to study tribological properties of styrene butadiene rubber composites under dry and wet conditions. It was shown that the SSBR filled with silicon dioxide nanoparticles significantly reduced both the friction coefficient and the wear against marble block. On the contrary, it exhibited an increased friction coefficient and wear under wet friction conditions due to the specific superior wet-skid resistance of silicon dioxide nanopartilce filled rubber composites, a good dispersion of silicon dioxide nanopartilce in the rubber matrix and strong interfacial adhesion between nanoparticles and rubber matrix. In addition, the influence of fillers dispersion and interfacial adhesion on friction and wear of styrene butadiene rubber composites was evaluated employing theoretical calculation, and the predicted results were in agreement with the experimental observations. © 2016 Wiley Periodicals, Inc. J. Appl. Polym. Sci. **2016**, *133*, 43589.

KEYWORDS: applications; composites; friction and wear; rubber; structure–property relations

Received 3 November 2015; accepted 27 February 2016

DOI: 10.1002/app.43589

INTRODUCTION

Abrasion resistance and wet-skid resistance, two of the main factors of tire treads contributing to their service lives and road safety, are mainly dependant on the tribological behavior between the tire treads and road pavement surfaces. Carbon black and silica, as a reinforcement agent, are conventional fillers that are widely used in the rubber industry. It is generally acknowledged that the dispersion of the carbon black (or silica) and interfacial interactions between the carbon black and rubber matrix are the key factors to determine the properties of vulcanized rubber composites.[1,2] Consequently, it is critically important, but often challenging, to enhance the overall performances of the rubber composites through improving the dispersion of the fillers and enhancing the interfacial interactions between the fillers and rubber matrix.

To date, considerable effort has been focused on investigating the influence of surface energies of fillers and interfacial interactions on thermodynamic and mechanical properties of different rubber composites. For example, Bharath *et al.* have studied the effect of interfacial energetic on dispersion and glass transition temperature in polymer composites, they revealed that the quantitative structure–properties relationships could be used to predict the morphological descriptors and changes in interface mobility. In turn, be used to construct finite element models of nanoparticle dispersions in matrices with the corresponding interphase properties.[3] Stöckelhuber *et al.* have studied the impact of surface energetic properties of filled elastomers on mechanical characteristics of rubber materials, such as flocculation, static and dynamic mechanical properties, and large-strain behavior. They discovered that an absorbed layer of immobilized polymer chains at the solid filler surface formed, and this process depended on the surface energies of filler and rubber matrix. Fillers with a low filler/polymer interaction showed low activation energy in the nonlinear amplitude behavior; whereas

Additional Supporting Information may be found in the online version of this article.

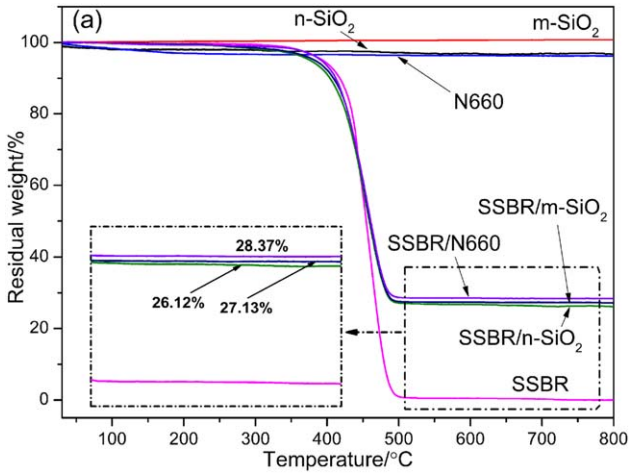

Figure 1. TGA thermogram of m-SiO_2, n-SiO_2, N660, pure SSBR, and SSBR composites with different fillers. [Color figure can be viewed in the online issue, which is available at wileyonlinelibrary.com.]

a coupling reaction of the solid filler surface to the polymer chains by means of a bifunctional silane is enhancing the formation of a stable interphase around the filler particles.[4] Furthermore, based on molecular dynamics simulations, the detailed structural analysis of the interphase molecules in the rubber composites has been intensively studied to develop structure–properties relationships. The important findings demonstrated that the nonbonding interaction between the nanoparticle and matrix contribute to the filler size dependency in elastic stiffness; the covalent grafting only leads to the gradually and long-range variation of the size dependent elastic moduli and does not contribute to size effect itself.[5,6]

To enhance the dispersion of fillers and strengthen the interfacial interaction between the filler and rubber matrix, on the one hand, many researchers have used various types of covalent and noncovalent modification in the manufacture of rubber composites.[7–11] On the other hand, various types of novel fillers were developed, such as cellulose nanocrystal,[12] modified lignosulfonates,[13] expanded graphite and graphene oxide,[14,15] carbon nanotube,[16,17] and nanosprings.[18] However, at present, still little available information about friction and wear properties of these novel rubber composites under both dry and wet conditions has been achieved. Therefore, an indepth investigation on the abrasion resistance and wet-skid resistance properties is needed, especially in understanding and quantifying the characteristics that lead to observed tribological properties being crucial to optimally design rubber materials, and these properties have largely depended on the dispersion of fillers and interfacial interaction between the filler and rubber. In this study, three kinds of rubber composites containing Si69 treated fumed silica, commercial silica, and carbon black (N660) fillers were prepared by conventional mixing technique. The morphological structure, dispersion of the filler, thermal stability, glass transition characteristics, and mechanical properties of three rubbers filled with different fillers were investigated, respectively. Besides, the interfacial adhesion, friction, wear properties of the rubbers and their relationships were analyzed in detail. It is expected that these experimental results can provide the theoretical basis and novel design for green tire tread material with improved wear resistance, wet skid resistance and low rolling resistance.

EXPERIMENTAL

Materials

Solution styrene butadiene rubber (SSBR, SE-G1122) matrix (styrene content of 25%) was supplied by Sumitomo Chemical, Japan. Acetone and glycerol were obtained from Shanghai Chemical. Carbon black (N660) was purchased from Tianjin Qiushi Chemical. Silica with a diameter of 10 nm (n-SiO_2), silicon dioxide with a diameter of 11 μm (m-SiO_2), silane coupling agent Si69 [*bis*-(γ-triethoxysilylpropyl)-tetrasulfide], zinc oxide (ZnO), stearic acid, xylene and sulfur (S_8) were purchased from Xilong Chemical. Diphenyl guanidine (DPG) and *N*-cyclohexyl-2-benzothiazolylsulfenamide (CBS) were bought from Aladdin Industrial Corporation and Tokyo Chemical Industry, respectively. All chemicals were used as received.

Preparation of SSBR Composites

The formulations of all SSBR composites with different fillers were using a two-roll mill [(S)XK 100B, Changzhou Dongfang Huayang Machinery Factory, China] and subjected to compression at 160 °C under 10 MPa pressure with the optimum curing time (t_{90}, determined by a vulcameter) by employing a plate vulcanizing machine (XLB-D, Huzhou Hongqiao Rubber Machinery, China). The basic formula of the composite was as follows: SSBR 100 phr; zinc oxide 2.5 phr; stearic acid 1 phr; diphenyl guanidine 1.5 phr; *N*-cyclohexyl-2-benzothiazolylsulfenamide 1.4 phr; sulfur 1.4 phr, and fillers. In this context, n-SiO_2, m-SiO_2, and N660 were chosen as fillers (35 phr), respectively, which the composites are marked as SSBR/m-SiO_2, SSBR/n-SiO_2, and SSBR/N660. The modified n-SiO_2 and m-SiO_2 using silane coupling agent Si69 (0.5 phr) are marked as n-SiO_2/Si69, m-SiO_2/Si69, respectively.

Tensile Strength Measurements

The tensile strength measurements of the SSBR/n-SiO_2, SSBR/m-SiO_2, and SSBR/N660 were carried out with a tensile

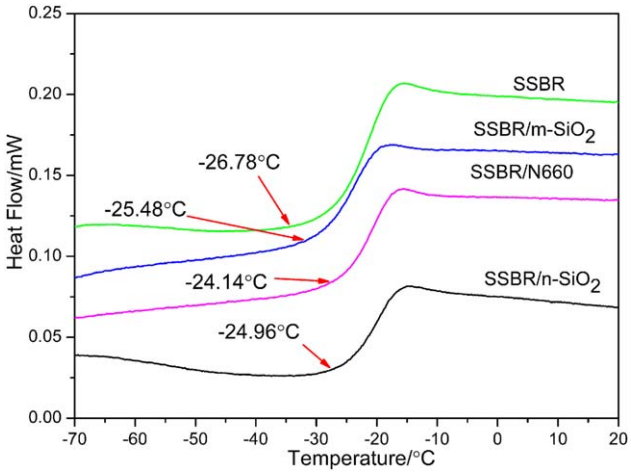

Figure 2. DSC curves of pure SSBR and SSBR composites with different fillers. [Color figure can be viewed in the online issue, which is available at wileyonlinelibrary.com.]

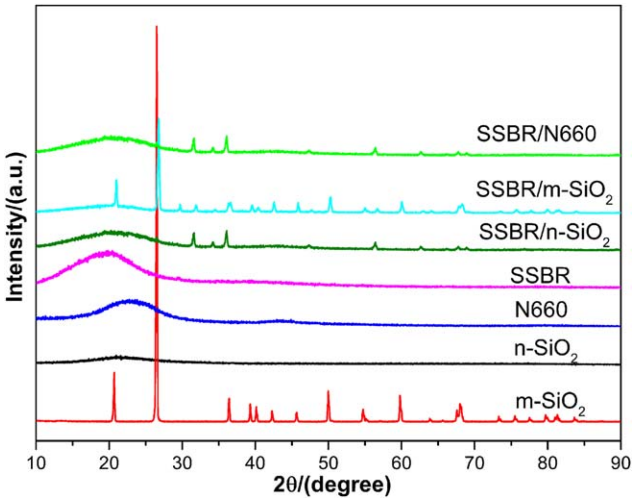

Figure 3. X-ray diffractograms of *m*-SiO_2, *n*-SiO_2, N660, pure SSBR, and SSBR composites with different fillers. [Color figure can be viewed in the online issue, which is available at wileyonlinelibrary.com.]

apparatus (WDW-200, Shandong Zhongyi Machine, China) at 25 °C according to Chinese Standard GB/T528-1998. The samples were subjected to a stress–strain test at a crosshead speed of 500 mm/min at room temperature. The tensile properties (elongation, modulus, and tensile strength) were deduced from the stress–strain curve. For each composite, five measurements were averaged.

Thermogravimetric Analysis

Thermogravimetric analysis (TGA) of different filled SSBR composite was performed on a simultaneous thermal analyzer (Netzsch STA449F3, Germany) from ambient temperature to 800 °C at a rate of 10 °C/min under N_2 atmosphere.

DSC Analysis

The glass-transition temperature (T_g) of the compounds and SSBR composites were investigated with DSC (DSC200F3, Netzsch, Germany). All samples were cooled to −80 °C at 10 °C/min and reheated up to 80 °C at 10 °C/min.

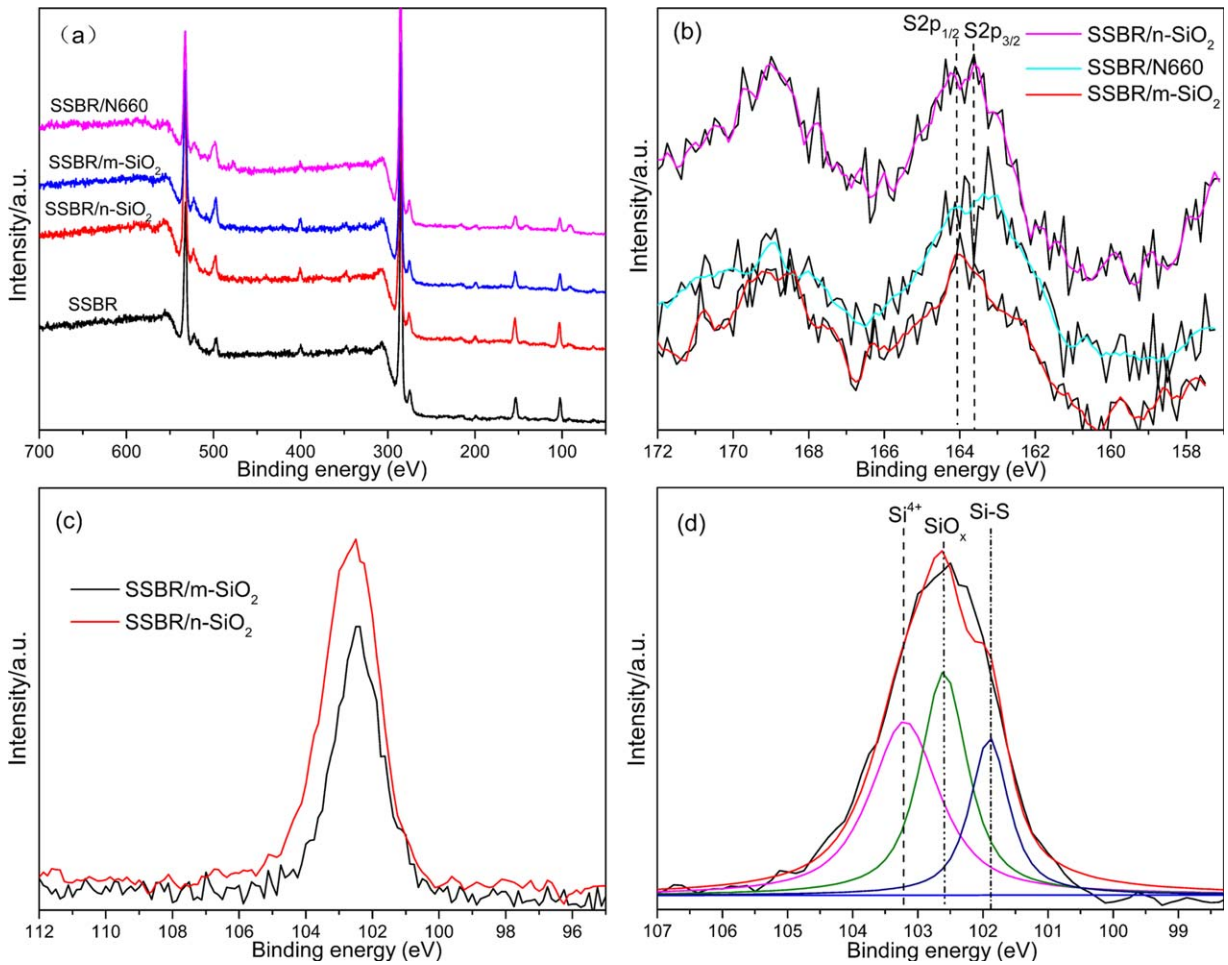

Figure 4. XPS spectra of pure SSBR and SSBR composites with different fillers (a), the S2p XPS spectra of the SSBR composites (b), the Si2p XPS spectra of the SSBR/*m*-SiO_2 and SSBR/*n*-SiO_2 (c), and the Si2p of SSBR/*n*-SiO_2 (d). [Color figure can be viewed in the online issue, which is available at wileyonlinelibrary.com.]

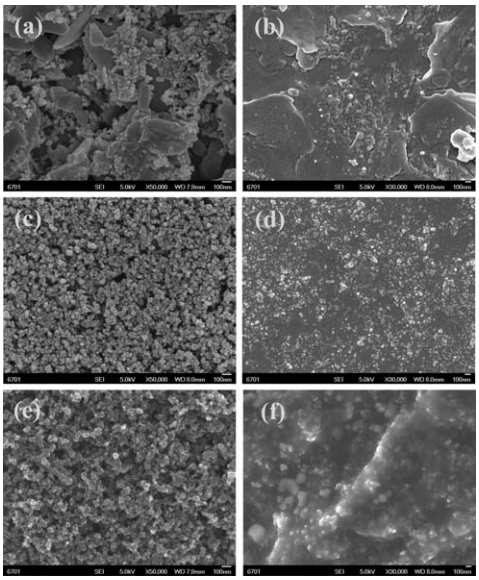

Figure 5. FESEM images of m-SiO_2 (a) and SSBR/m-SiO_2 (b), n-SiO_2 (c) and SSBR/n-SiO_2 (d), N660 (e) and SSBR/N660 (f).

X-ray Diffraction Measurement

Wide-angle X-ray diffraction measurement (XRD, Rigaku, Japan) was carried out to characterize the structures of m-SiO_2, n-SiO_2, and the SSBR composites with Cu Kα radiation (40 kV, 100 mA, $\lambda = 0.154$ nm) over the angular range $2\theta = 10$–$80°$, with a step size of 2°/min.

TEM Measurement

Transmission electron microscopy (TEM) images were recorded on JS*M*-1200EX at 200 kV, The m-SiO_2, n-SiO_2, and carbon black (N660) powders were dropped onto carbon support film which tops on a copper grid, and the solvent was allowed to evaporate before observation. The ultrathin section specimens of SSBR composites for TEM observation were cut on a Leica Ultracut-R ultramicrotome at −80 °C in nitrogen atmosphere.

SEM Measurement

Field-emission scanning electron microscopy (FESEM) and scanning electron microscopy (SEM) analyses of the samples, worn surface and wear debris of the SSBR composites were carried on a JS*M*-6701F and JS*M*-5600LV microscopy, respectively. The sample was sputtered with a thin layer of gold prior to the

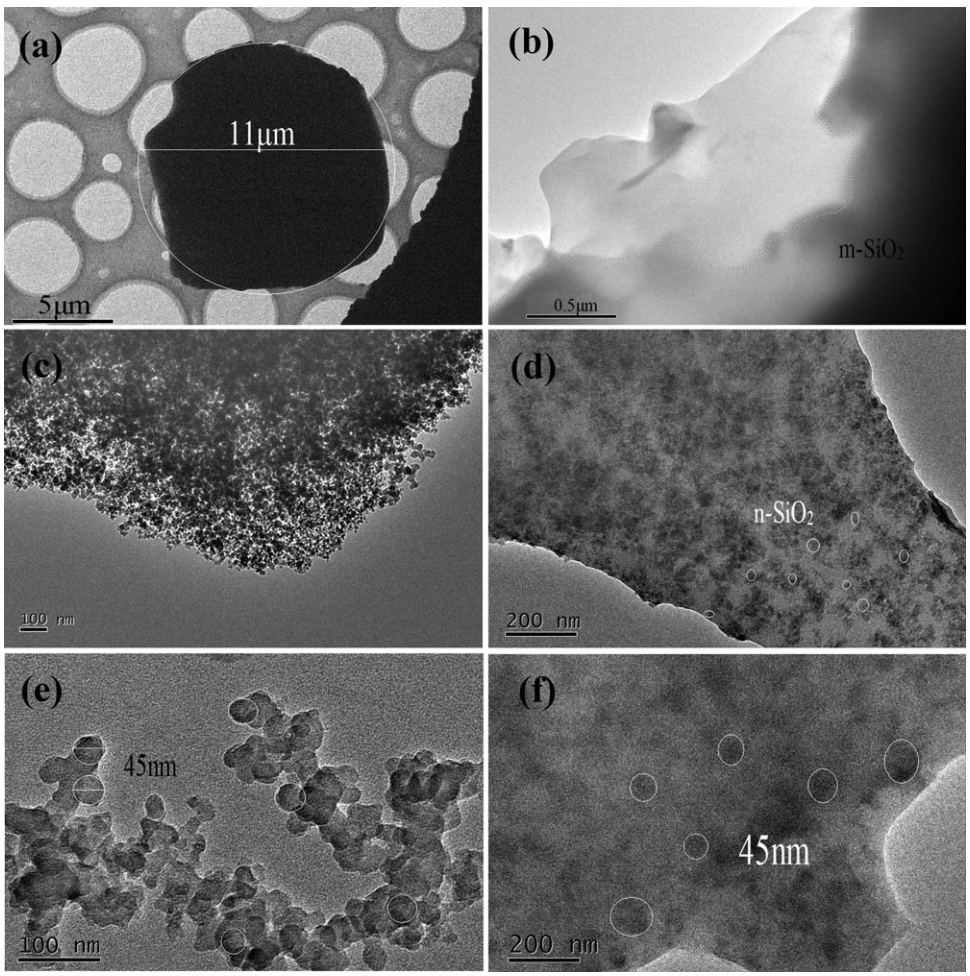

Figure 6. TEM photographs of m-SiO_2 (a) and SSBR/m-SiO_2 (b), n-SiO_2 (c) and SSBR/n-SiO_2 (d), N660 (e), and SSBR/N660 (f).

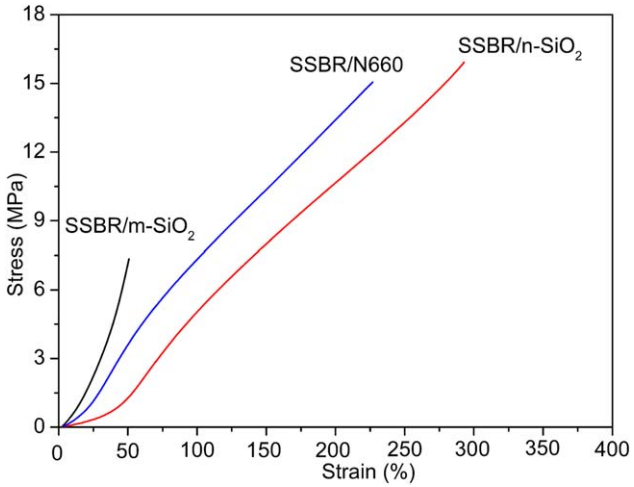

Figure 7. Typical stress–stain curves of the SSBR composites with different fillers. [Color figure can be viewed in the online issue, which is available at wileyonlinelibrary.com.]

measurement, except for carbon black powder (N660) and SSBR/N660 specimen, and the measurement were performed at an accelerating voltage of 5 and 20 kV. Energy dispersive spectrometer (EDS) was attached to the scanning electron microscope.

XPS Analysis

X-ray spectroscopy (XPS) analysis was carried out on a Kratos Axis Ultra DLD equipped with Al Kα radiation source (1486.6 eV).

Dynamic Mechanical Analysis

Dynamic mechanical analysis (DMA) was performed on a DMA/SDTA861e instrument under a tensile mode with a dynamic strain of 0.5%. The samples were scanned from −80 to 80 °C, and the frequency and heating rate were fixed at 1 Hz and 3 °C/min, respectively.

Static Contact Angles Measurement

Static contact angles were measured using the Krüss DSA100 drop shape analysis system (Krüss GmbH, Germany). The contact angle was recorded within 2 s after liquid deposition. Water and glycerol were used as the test liquids. To prepare the samples for the contact angle measurements, two different SiO_2 and carbon black (N660) powders were pasted to the thin scotch tape, and SSBR was dissolved in xylene, coated on to a glass slide, and then dried to form a film.

Roughness Analysis

The surface roughness of filled SSBR samples under dry friction and water existence conditions were also investigated employing dual-mode three-dimensional surface profiler (NanoMap-D, APE).

Friction and Wear Behaviors

The tribological tests were conducted on a M*M*-200 ring-block frictional tester, a marble block (30 ± 0.l mm in length, 6 mm in width, and 7 ± 0.1 mm in thicknesses) was used as the counterparts, with arithmetic average roughness of 7.0 μm. The rubber sample was fasten on to the stainless steel ring (Ø40 mm). All experiments were carried out in the conditions (temperature: 15–25 °C, humidity: 8–15%, testing time: 60 min, rotational speed: 200 r/min) under dry friction and water-existed conditions, and the sliding tests were run at normal loads of 50, 60, 70, 80, 90, and 100 N. The SSBR composites were ultrasonically cleaned in acetone, dried, and weighted using an analytic balance (ME204E, measurement accuracy: 0.0001 g) before and after testing, the wear rate was calculated with the following eq. (1):

$$\text{Wear rate}\% = \frac{m_o - m_f}{m_o} \times 100\% \quad (1)$$

where m_f is the final mass after test; m_o is the original mass before test. All the experiments were carried out in triplicate.

RESULTS AND DISCUSSION

Figure 1 presents the thermal degradation properties of the pure SSBR and filled composites. As can be seen from the results, there is a little weight loss at initial temperature, which is due to the loss of water moisture. It is also found that the filled SSBR composites have similar degradation tendency and thermal stability. According to the curves of the weight loss of the SSBR/*m*-SiO_2, SSBR/*n*-SiO_2, and SSBR/N660, the residual materials in the SSBR composites are 27.13, 26.12, and 28.37 wt % after 500 °C, respectively.

The DSC curves of pure SSBR and SSBR composites with different fillers are shown in Figure 2, from which the glass transition temperatures (T_g) can be obtained according to the half step method. The pure SSBR has a T_g at about −26.78 °C, which is similar to previous reported.[19] With *m*-SiO_2, *n*-SiO_2, N660 being massively added in the SSBR, the T_g of the SSBR/*m*-SiO_2, SSBR/*n*-SiO_2, and SSBR/N660 slightly increase compared to the pure SSBR, and especially the T_g of the SSBR/*n*-SiO_2 and SSBR/N660 shifts to higher temperature of about −24.96 and −24.14 °C, respectively. These results could be explained that the silica and carbon black embedded crosslinked network,

Table I. Tensile Properties of the SSBR Composites with Different Fillers

Composites	Ultimate tensile strength (MPa)	Elongation at break (%)	Stress at 100% strain (MPa)	Stress at 200% strain (MPa)
SSBR/*m*-SiO_2	7.4	176.3	-	-
SSBR/*n*-SiO_2	16.0	382.2	3.6	9.8
SSBR/N660	15.1	361.3	2.3	7.7

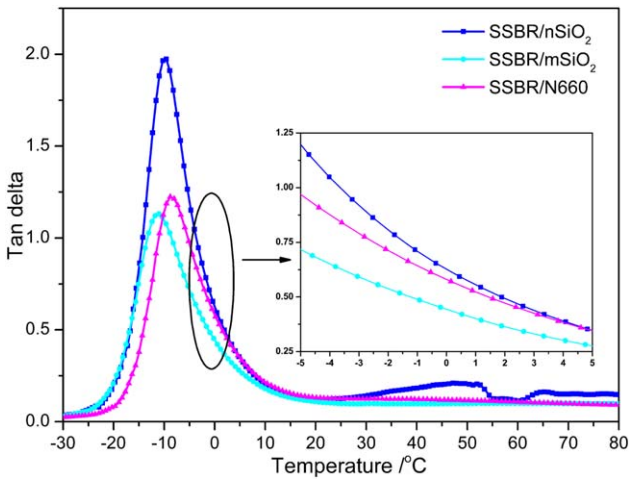

Figure 8. Mechanical loss factor (tan δ) as a function of temperature for SSBR/*m*-SiO_2, SSBR/*n*-SiO_2, and SSBR/N660 composites. [Color figure can be viewed in the online issue, which is available at wileyonlinelibrary.com.]

limiting the segment movement of chains, which caused the increase in the glass transition temperature of the composites.

The XRD profiles of *m*-SiO_2, *n*-SiO_2, N660, pure SSBR, and SSBR composites with different fillers are presented in Figure 3. A broaden peak is observed in the *n*-SiO_2 and SSBR/*n*-SiO_2 composites, indicating the existence of amorphous silica.[20] Similarly, the other peaks cannot be found in the SSBR/N660 sample except for the peaks of the ZnO, corresponding to (100), (002), and (101) lattice planes of ZnO wurtzite hexagonal structure,[21] indicating that only the highly disordered structure of carbon black N660 exists in the SSBR matrix. In addition, the XRD patterns show that the crystal structure of *m*-SiO_2 was mostly preserved and not affected significantly in SSBR matrix. These results imply that three fillers have different phase constitution in vulcanized SSBR matrix, and the highly ordered crystal structure of *m*-SiO_2 is still preserved in the rubber matrix. XPS was employed for further confirming the composites and structure changes of vulcanized SSBR samples, as shown in Figure 4. The S2p XPS spectrum [Figure 4(b)] consists of two peaks at 163.8 and 163.4 eV, corresponding to the $2p_{1/2}$ and $2p_{3/2}$ orbitals of S nanocrystals.[22] After vulcanization, the peak at about 169 eV is present, proving the existence of S ions with −2 valency in the SSBR composites.[23] Figure 4(d) shows the XPS signal from the silicon (Si) 2p spectral region for the SSBR/*n*-SiO_2 composite, corresponding to the peaks of Si ions with +4 valency at 103.3 eV and Si—S bond at 101.9 eV, indicating that the small amount of Si—S bond was existed in the SSBR/*n*-SiO_2 composite.

Table III. Theoretical Quantitative Predictors for Filler–Rubber Adhesion (W_a), Filler Flocculation (ΔW_a) and Work of Spreading (W_s)

	SSBR/*m*-SiO_2	SSBR/*n*-SiO_2	SSBR/N660
W_a (mJ/m^2)	18.888	33.406	14.810
ΔW_a (mJ/m^2)	35.436	37.514	29.874
W_s (mJ/m^2)	−16.408	−1.890	−20.486

The surface appearances and dispersion of fillers in SSBR matrix were then investigated by FESEM and TEM, as shown in Figures 5 and [6]. From the FESEM and TEM images shown in Figures 5(b) and 6(b), it can be observed that the *m*-SiO_2 particles are not uniformly dispersed and severely agglomerated in rubber matrix. As expected, the *n*-SiO_2 and carbon black N660 fillers are well dispersed in the rubber matrix, and especially the *n*-SiO_2 exhibits the best dispersion in rubber matrix compared with *m*-SiO_2 and N660 fillers attributing to the smallest particles size of *n*-SiO_2 nanoparticles, which is less than 10 nm, and corresponding to 45 nm for N660 particles.

The mechanical properties of SSBR/*m*-SiO_2, SSBR/*n*-SiO_2, and SSBR/N660 composites were characterized by tensile tests. Figure 7 shows the typical engineering stress–strain curves of the composites with different fillers. Tensile properties of the composites were summarized in Table I. The ultimate tensile strength of SSBR/*m*-SiO_2 composites is 7.4 MPa. For SSBR/*n*-SiO_2 composites, the ultimate tensile strength and stress at 100% strain were improved to 15.8 and 4.3 MPa, and for SSBR/N660 composites, corresponding to 15.1 and 7.5 MPa, respectively. Thus, the mechanical properties of SSBR/*n*-SiO_2 composites are better than those of SSBR/*m*-SiO_2 and SSBR/N660 composites, and the main reason is that the interaction between the modified SiO_2 nanoparticles and SSBR macromolecular chains is strong enough because of the high dispersion and grafted amount of SiO_2 nanoparticles, that is why the SSBR/*n*-SiO_2 samples processes excellent tensile strength. Furthermore, in Figure 8, the tan δ values of the composites containing three kinds of fillers are plotted against temperature. The result shows that, the glass transition region (−25 °C from to 8 °C) is observed in the curves of tan δ versus temperature. For SSBR/*n*-

Table II. Contact Angles and Surface Energies of SSBR and Varied Fillers

Sample	Water (°)	Glycerol (°)	γ_s^d (mJ/m^2)	γ_s^p (mJ/m^2)	γ_s (mJ/m^2)
SSBR	93.4	105.1	1.336	16.312	17.648
m-SiO_2	5.0	73.9	43.586	34.324	77.910
n-SiO_2	104.3	99.0	7.044	4.423	11.467
m-SiO_2/Si69	110.5	105.0	7.017	2.497	9.514
n-SiO_2/Si69	122.1	88.0	6.025	11.787	17.812
N660	121.2	117.4	2.877	1.817	4.694

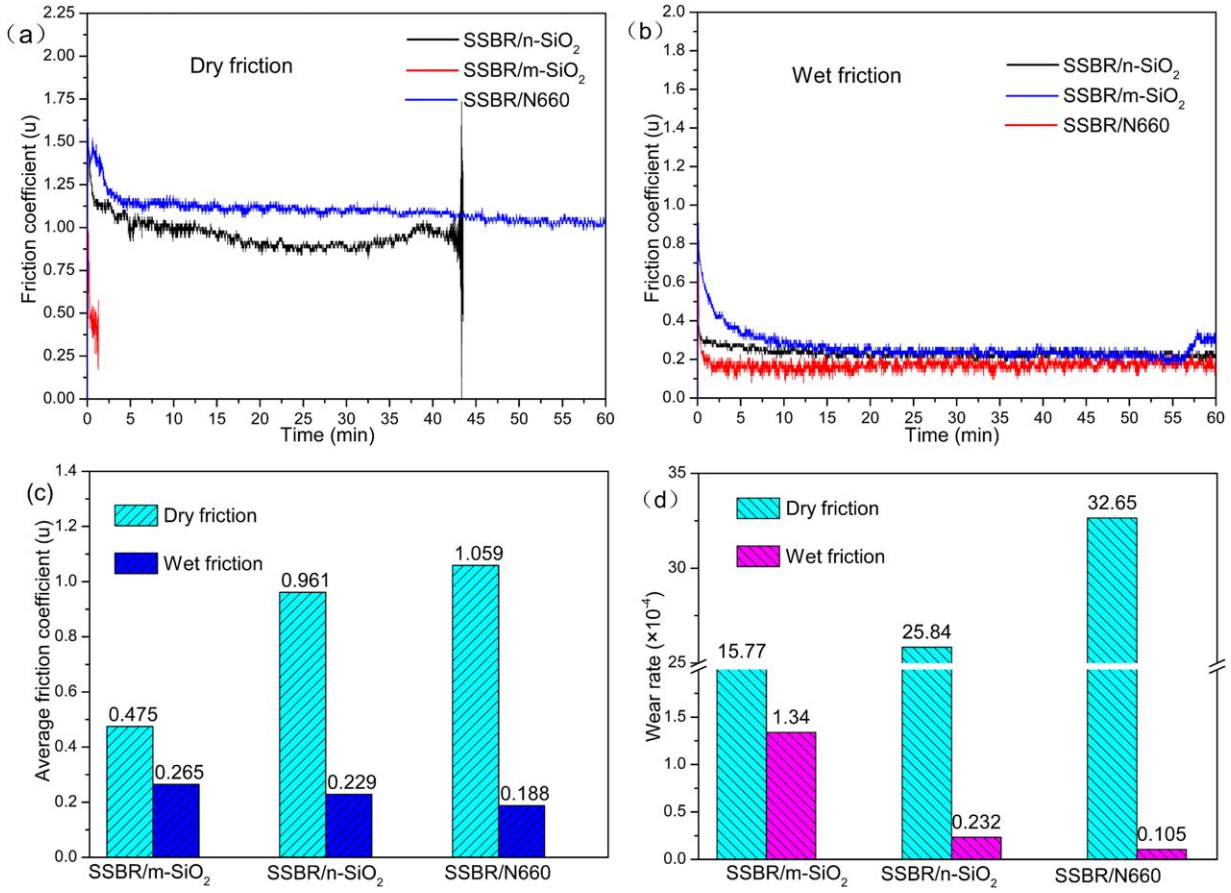

Figure 9. Comparison of the friction and wear behaviors of SSBR filled with different filler against marble block under dry (a) and wet (b) conditions and the average friction coefficients (c), and wear rate (d) of the rubber-reinforced composites under loading of 80 N. [Color figure can be viewed in the online issue, which is available at wileyonlinelibrary.com.]

SiO_2 composite, the tan δ at 0 °C was higher than that of SSBR/*m*-SiO_2 and SSBR/N660 composites, indicating that the *n*-SiO_2 filled rubber composites have excellent wet-skid resistance.

From the above structural analysis results and mechanical performance, it can be concluded that the nanoparticle-filled SSBR, i.e., *n*-SiO_2, was well dispersed in the SSBR matrix, and the Si69 modified surface of *n*-SiO_2 provided effective adhesion at the filler–matrix interface. In particular, when vulcanized SSBR matrix was reinforced with modified SiO_2 nanoparticles, it shows a significant increase in the tensile strength and wet-skid resistance for SSBR/*n*-SiO_2 composite compared to SSBR/*m*-SiO_2 composite.

Theoretically Quantitative Predictors for Dispersion and interfacial interaction in SSBR Composites

It is difficult to directly observe the influence of fillers dispersion and interfacial adhesion on friction and wear behavior of SSBR composites. However, in rubber composites, the wettability of the filler in rubber, the interfacial adhesion between filler and rubber as well as the reagglomeration of filler are mainly driven by surface energies of filler and rubber matrix,[3] which are useful in providing a better understanding of the influence of fillers dispersion and interfacial adhesion on friction and wear performance. Here, we mainly use Fowkes' model to calculate the surface energies of the fillers and pure SSBR matrix, as described in eqs. 2 and 3.[24]

$$\gamma_L(1+\cos\theta)=2\left(\sqrt{\gamma_L^d\gamma_S^d}+\sqrt{\gamma_L^p\gamma_S^p}\right) \quad (2)$$

$$\gamma_S=\gamma_S^d+\gamma_S^p;\ \gamma_L=\gamma_L^d+\gamma_L^p \quad (3)$$

where θ is static contact angles between the samples (fillers and SSBR matrix) and water (or glycerol), γ_L^d and γ_L^p are the dispersive and polar components of the surface energies of the liquid; γ_S^d and γ_S^p are the dispersive and polar components of the surface energies of the solid; γ_L and γ_S are the total surface energies of the liquid and solid, respectively. Herein, the test liquids were water and glycerol. The γ_L^d and γ_L^p values for water are 21.8 and 51 mJ/m^2, and for glycerol are 34 and 30 mJ/m^2, respectively. The surface energies of the different fillers and pure SSBR were calculated by substituting the contact angles and surface energies of the test liquids into eqs. 2 and 3; images of the contact angle of water of materials are shown in Supporting Information Figure S1, the results are summarized in Table II. The surface energy of the pure SSBR matrix is determined to be 17.65 mJ/m^2, which is similar to the surface energy of SBR matrix in previous reports.[25]

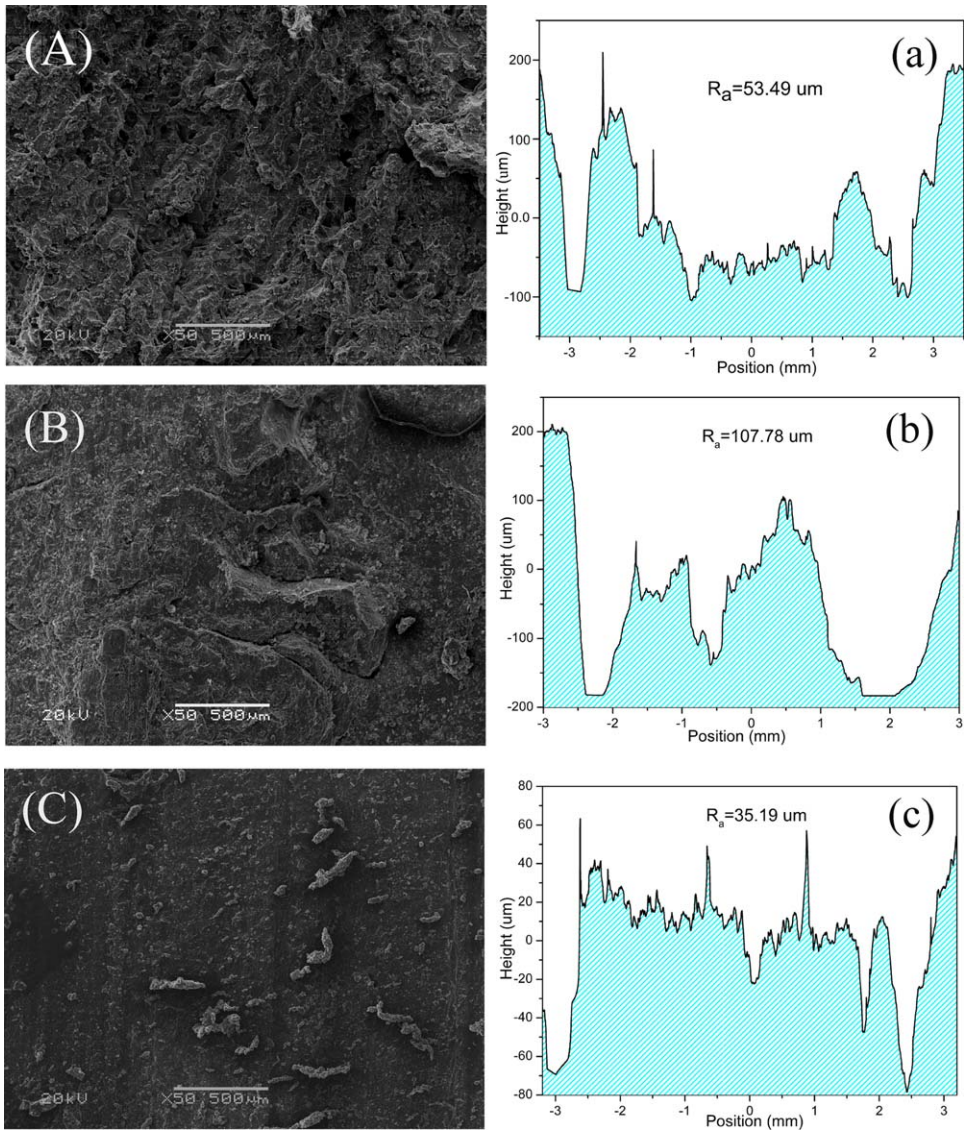

Figure 10. Morphology and 2D profiles of the worn surface for SSBR/*m*-SiO_2 (A), SSBR/*n*-SiO_2 (B), and SSBR/N660 (C) under the dry friction conditions (80 N); (a), (b), and (c) responding to morphologies of worn surface and roughness (a testing time of 2 min for SSBR/*m*-SiO_2 and 43 min for SSBR/*n*-SiO_2 composites because they are easy to wear out, a testing time of 60 min for SSBR/N660 composites). [Color figure can be viewed in the online issue, which is available at wileyonlinelibrary.com.]

According to Fowkes' model, the adhesive energy (W_a) between filler and rubber is given by:

$$W_a = 2\left(\sqrt{\gamma_F^d \gamma_R^d} + \sqrt{\gamma_F^p \gamma_R^p}\right) \tag{4}$$

where γ_F^d and γ_F^p are the dispersive and polar components of the surface energies of the fillers; γ_R^d and γ_R^p are the dispersive and polar components of the surface energies of the SSBR matrix.

Wang[26] and Stöckelhuber *et al.*[27] noted that the driving force for filler flocculation (ΔW_a) was determined by the change in potential energy when filler–filler and rubber–rubber interfaces are created from two filler–rubber interfaces, and the potential energy change can be effectively captured by the change in adhesive energy, which is the relative adhesion of filler to filler (W_{FF}) and rubber to rubber (W_{RR}) minus twice the adhesion of rubber to filler (W_{RF}) and a large value of ΔW_a means a large driving force for reagglomeration.

$$\Delta W_a = W_{FF} + W_{RR} - 2W_{RF} \tag{5}$$

$$\Delta W_a = 2\left(\gamma_F^d + \gamma_F^p\right) + 2\left(\gamma_R^d + \gamma_R^p\right) - 2\left(\sqrt{\gamma_F^d \gamma_R^d} + \sqrt{\gamma_F^p \gamma_R^p}\right) \tag{6}$$

Furthermore, the interfacial adhesion can be reflected in the mobility of the rubber chains at the interface, which is related to the work of spreading (W_s):

$$W_s = W_{RF} - W_{RR} \tag{7}$$

$$W_s = 2\left(\sqrt{\gamma_F^d \gamma_R^d} + \sqrt{\gamma_F^p \gamma_R^p}\right) - 2\left(\gamma_R^d + \gamma_R^p\right) \tag{8}$$

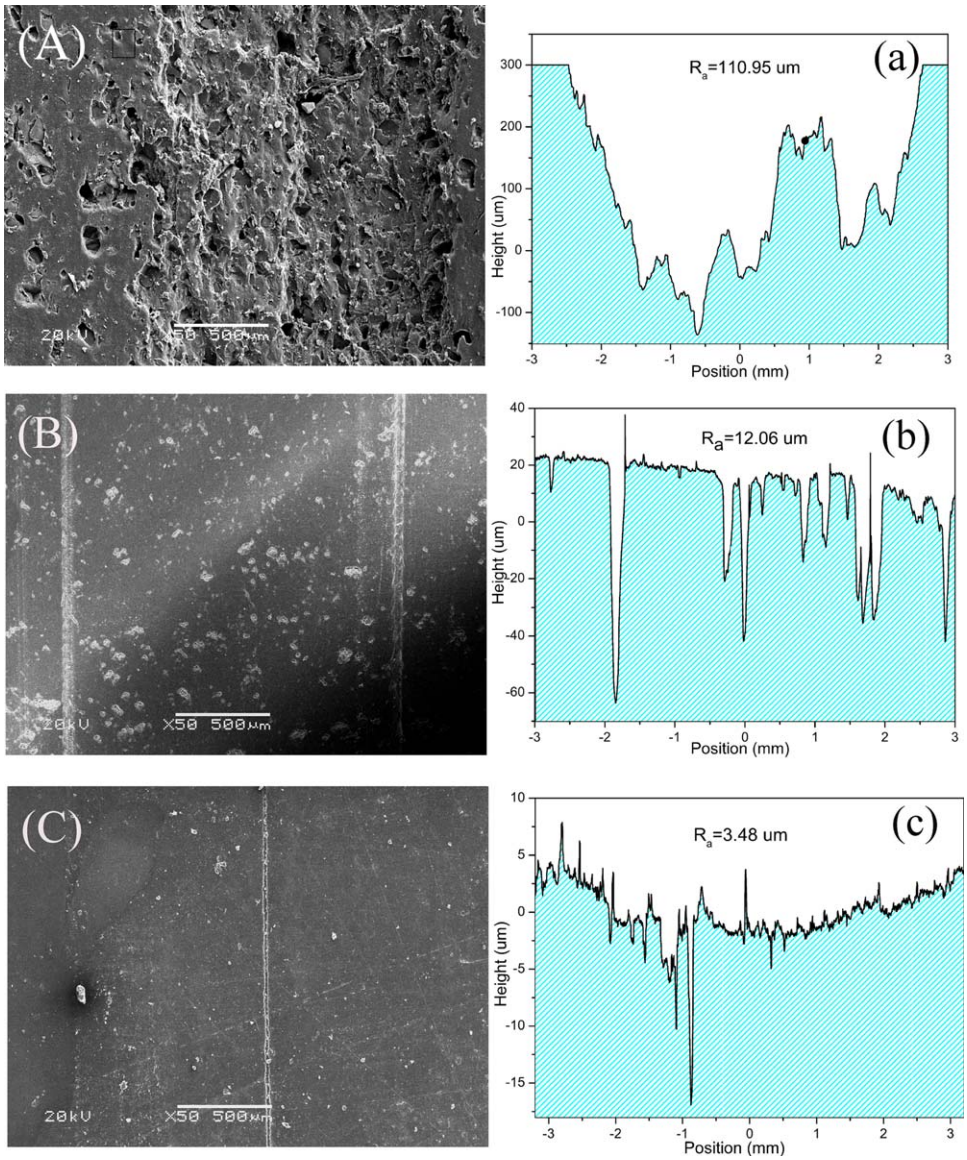

Figure 11. Morphology and 2D profiles of the worn surface for SSBR/*m*-SiO_2 (A), SSBR/*n*-SiO_2 (B), and SSBR/N660 (C) under the wet friction conditions (80 N); (a), (b), and (c) responding to morphologies of worn surface and roughness. [Color figure can be viewed in the online issue, which is available at wileyonlinelibrary.com.]

The larger the value of W_s, the stronger interfacial adhesion between the filler and rubber. It should be pointed out that the dispersion of N660 in SSBR matrix, as revealed by the SEM and TEM images, is still fairly uniform, although it is not as good as the dispersion of *n*-SiO_2 nanoparticles. On the basis of the values of W_a, the modified *n*-SiO_2 nanoparticles is expected to be stronger interfacial adhesion than modified *m*-SiO_2 and N660 being ascribed to the higher W_a value of *n*-SiO_2 in SSBR matrix. As shown in Table III, it was illustrated that the strongest interaction between the modified *n*-SiO_2 and SSBR matrix was occurred compared with the *m*-SiO_2 and carbon black N660. Regarding the values of ΔW_a, which is always positive, it means that the filler will inevitably reaggregate at elevated temperature. The value of ΔW_a is the highest for *n*-SiO_2 in SSBR matrix, indicating that modified *n*-SiO_2 nanoparticles tend to undergo severe reaggregation due to the great polar surface energy of modified SiO_2 nanoparticles. Compared with the values of SSBR/*m*-SiO_2, SSBR/N660, and SSBR/*n*-SiO_2, the value of ΔW_a for N660 is the lowest, implying that the reaggregation of the carbon black N660 is weakest among the modified micro-size SiO_2 particles, SiO_2 nanoparticles, and carbon black N660 particles in SSBR matrix. As mentioned above, the larger values of W_s suggested that the stronger interfacial interaction between filler and rubber, it is clear that the interfacial adhesion between the modified *n*-SiO_2 nanoparticles and SSBR matrix is superior to those between modified *m*-SiO_2, carbon black N660 and SSBR matrix, respectively.

Friction and Wear Performance of SSBR Composite Under Dry and Wet Conditions

Figure 9(a) and (b) show that, under the dry and wet conditions, the friction coefficient of SSBR/*m*-SiO_2, SSBR/*n*-SiO_2, and SSBR/N660 as a function of sliding times against a marble block

under a constant load of 80 N, and the effects of the others different loads on friction and wear were also studied [Supporting Information Figure S(2a–f)]. It shows that the SSBR/*m*-SiO_2 merely maintains low friction within 2 min, and then is worn out, which indicated that the poor dispersion of *m*-SiO_2 in SSBR matrix led to bad abrasive resistance. While for *n*-SiO_2 and carbon black based SSBR composites, the friction curves show significant differences from the SSBR/*m*-SiO_2 composite. Under dry friction condition, a low average friction coefficient and mass loss rate were obtained for SSBR/*n*-SiO_2 composites compared with the SSBR/N660 composites. Oppositely, a high average friction coefficient and mass loss rate were obtained under wet friction condition, as shown in Figure 9(c) and (d). This fact confirms that, generally, the wet-skid resistance of SSBR/*n*-SiO_2 composites was superior to the SSBR/N660 composites under the same conditions.

To better reveal the friction and wear behavior of the reinforced SSBR composites, an SEM examination of the worn surface was carried out, under dry and wet friction conditions. Figures 10 and 11 show the surface morphologies of worn track and roughness for the SSBR/*m*-SiO_2 (A and a), SSBR/*n*-SiO_2 (B and b), and SSBR/N660 (C and c) at the load of 80 N, respectively. Larger tearing and grooves were apparent on the surface of SSBR/*m*-SiO_2 and SSBR/*n*-SiO_2 composites, while the worn track on the SSBR/N660 surface was relatively smooth and displayed the small tearing, which was the typical morphology of the severe abrasive wear. The worn surface roughness of the SSBR/N660 (35.19 μm) was obviously lower than those of SSBR/*m*-SiO_2 (53.49 μm) and SSBR/*n*-SiO_2 (107.78 μm) composites. Effect of load on the morphology of worn surface under dry friction condition was also observed, the results indicated that the worn surface of SSBR/*n*-SiO_2 at lower load was smoother than that at the higher load, and the worn surface morphology of SSBR/N660 exhibited serious tearing and spalling at the different loads (Supporting Information Figures S3 and S4). Combining with EDS elemental maps taken from the worn surface of the filled SSBR composites (Supporting Information Figure S5), these directly proved that it was impossible to form a new compounds on the worn surface, and the mass loss rate of SSBR/N660 was lower than those of SSBR/*m*-SiO_2 and SSBR/*n*-SiO_2 composites at the different loads. Furthermore, the surface morphologies of worn debris for SSBR/*m*-SiO_2 and SSBR/*n*-SiO_2 composites were observed (Supporting Information Figures S6 and S7), it could be found that the debris at lower loads was shorter and narrower than those at higher loads for SSBR/*n*-SiO_2 and SSBR/N660 samples, which indicated that the wear mechanisms at the lower and higher loads were different. The abrasive wear is the main wear mechanism at lower loads, and the adhesive and fatigue wear play an important role at higher loads. Under wet friction condition, it was interesting to note that the main wear traces for SSBR/*n*-SiO_2 and SSBR/N660 composites were caused by the surface protuberances of counterparts.[28] The value of the roughness of the SSBR/*n*-SiO_2 and SSBR/N660 are 12.06 and 3.48 μm (Supporting Information Figures S8 and S9), respectively. Abrasive wear was the main wear mechanism. Particularly, the worn surface of SSBR/*m*-SiO_2 samples exhibited the deepen grooves even if at the short sliding times, for example, within 2 min, revealing the different wear behavior, and the value of roughness was 110.95 μm (Supporting Information Figure S10), which was consistent with the results of mechanical measurements previously.

CONCLUSIONS

In this work, three kinds of filled rubber composites were fabricated by conventional mixing technique. Field-emission scanning electron microscopy and transmission electron microscopy revealed that, *n*-SiO_2 exhibited much better dispersion in the SSBR matrix compared with the *m*-SiO_2 and carbon black N660. In addition, the influence of the filler surface chemistry on the dispersion of fillers and interfacial adhesion in the SSBR matrix were quantified by theoretical calculation, and with experimental tests. It could draw a conclusion that the *n*-SiO_2 nanoparticles exert a great good dispersion in the SSBR matrix and strong interfacial interaction between the modified surface of SiO_2 nanoparticles and SSBR matrix, resulting in greater enhancement of the mechanical properties and tribological performance. This present work is expected to provide significant insight into the relationships among dispersion of fillers and interfacial adhesion and the tribological properties as well as mechanical properties of the SSBR composites; this article provides a foundation for the preparation of high-performance tire tread composites from the perspective of the rational choice of reinforcing fillers.

ACKNOWLEDGMENTS

This work was supported by National Basic Research Program of China, Grant No. 2015CB654700 (2015CB654705) and the Chinese Academy of Sciences.

REFERENCES

1. Valentín, J. L.; Mora-Barrantes, I.; Carretero-González, J.; López-Manchado, M. A.; Sotta, P.; Long, D. R.; Saalwachter, K. *Macromolecules* **2009**, *43*, 334.
2. Baeza, G. P.; Genix, A. C.; Degrandcourt, C.; Petitjean, L.; Gummel, J.; Schweins, R.; Couty, M.; Oberdisse, J. *Macromolecules* **2013**, *46*, 6621.
3. Natarajan, B.; Li, Y.; Deng, H.; Binson, L. C.; Schadler, L. S. *Macromolecules* **2013**, *46*, 2833.
4. StÖckelhuber, K. W.; Svistkov, A. S.; Pelevin, A. G.; Heinrich, G. *Macromolecules* **2011**, *44*, 4366.
5. Froltsov, V. A.; Klüppel, M.; Raos, G. *Phys. Rev. E* **2012**, *86*, 041801.
6. Yang, S.; Choi, J.; Cho, M. *ACS Appl. Mater. Interfaces* **2012**, *4*, 4792.
7. Kim, Y. J.; Ha, S. W.; Jeon, S. M.; Yoo, D. W.; Chun, S. H.; Sohn, B. H.; Lee, J. K. *Langmuir* **2010**, *26*, 7555.
8. Cheng, H. K. F.; Sahoo, N. G.; Tan, Y. P.; Pan, Y.; Bao, H.; Li, L.; Chan, S. H.; Zhao, J. *ACS Appl. Mater. Interfaces* **2012**, *4*, 2387.

9. Valentín, J. L.; Posadas, P.; Marcos–Fernández, A.; Lbarra, L.; Rodríguez, A. *J. Appl. Polym. Sci.* **2006**, *99*, 3222.
10. Liu, X.; Zhao, S.; Yang, Y.; Zhang, X.; Wu, Y. *Polym. Adv. Technol.* **2009**, *20*, 818.
11. Li, Y.; Han, B.; Wen, S.; Lu, Y.; Yang, H.; Zhang, L.; Liu, L. *Compos. A: Appl. Sci. Manufact.* **2014**, *62*, 52.
12. Kargarzadeh, H.; Sheltami, R. M.; Ahmad, I.; Abdullah, I.; Dufresne, A. *Polymer* **2015**, *71*, 51.
13. Bahl, K.; Jana, S. C. *J. Appl. Polym. Sci.* **2014**, *131*, 40123.
14. Balachandran, N. A.; Philip, K.; Rani, J. *Euro. Polym. J.* **2013**, *49*, 247.
15. Mao, Y.; Wen, S.; Chen, Y.; Zhang, F.; Panine, P.; Chan, T. W.; Zhang, L.; Liang, Y.; Liu, L. *Scientific Rep.* **2013**, *3*, 2508.
16. Le, H. H.; Abhijeet, S.; Ilisch, S.; Klehm, J.; Henning, S.; Sarkawi, S. S.; Dierkes, W.; Das, A.; Fischer, D.; Stöckelhuber, K. W.; Wiessner, S.; Khatiwada, S. P.; Adhikari, R.; Pham, T.; Heinrich, G.; Radusch, H. J. *Polymer* **2014**, *55*, 4738.
17. Nair, S. T.; Vijayan, P. P.; Xavier, P.; Bose, S.; George, S. C.; Thomas, S. *Compos. Sci. Technol.* **2015**, *116*, 9.
18. Liu, J.; Lu, Y. L.; Tian, M.; Li, F.; Shen, J.; Gao, Y.; Zhang, L. *Adv. Funct. Mater.* **2013**, *23*, 1156.
19. Malas, A.; Das, C. K. *Polym. Eng. Sci.* **2014**, *54*, 33.
20. Tu, J.; Yuan, Y.; Zhan, P.; Jiao, H.; Wang, X.; Zhu, H.; Jiao, S. *J. Phys. Chem. C* **2014**, *118*, 7357.
21. Rathnayake, W.; Ismail, H.; Baharin, A.; Bandara, I. M. C. C. D.; Rajapakse, S. *J. Appl. Polym. Sci.* **2014**, *131*, 39601.
22. Yu, Y.; Rowland, C. E.; Schaller, R. D.; Korgel, B. A. *Langmuir* **2015**, *31*, 6886.
23. Niu, W.; Xu, H.; Guo, Y.; Li, Y.; Ye, Z.; Zhu, L. *Phys. Chem. Chem. Phys.* **2015**, *17*, 16705.
24. Fowkes, F. M. *J. Phys. Chem.* **1963**, *67*, 2538.
25. Tang, Z.; Zhang, L.; Feng, W.; Guo, B.; Liu, F.; Jia, D. *Macromolecules* **2014**, *47*, 8663.
26. Wang, M. *J. Rubber Chem. Technol.* **1998**, *71*, 520.
27. Stöckelhuber, K. W.; Das, A.; Jurk, R.; Heinrich, G. *Polymer* **2010**, *51*, 1954.
28. Hong, C. K.; Kim, H.; Ryu, C.; Nah, C.; Huh, Y.; Kaang, S. *J. Mater. Sci.* **2007**, *42*, 8391.